COBEM 2021 26th International Congress of Mechanical Engineering
November 22-26, 2021, Virtual Congress, Brazil

COB-2021-0775
EVALUATION OF CEMENTED CARBIDE/HIGH-SPEED STEEL COMPOSITE SINTERED BY PECS

Daniella Gualberto Caldeira de Paula
João Paulo Luiz Grisotto Alves
Ailana Kröhling Uliana
Mariane Gonçalves de Miranda
Marcelo Bertolete Carneiro
Federal University of Espírito Santo, Department of Mechanical Engineering, 29075-910, Vitória/ES, Brazil
daniella_gualberto@hotmail.com; jpluizalves13@yahoo.com.br; ailanauliana@gmail.com; mariane.miranda@edu.ufes.br; marcelo.b.carneiro@ufes.br

Izabel Fernanda Machado
*University of São Paulo, Polytechnic School, Department of Mechatronics Engineering and Mechanical Systems, 05508-900, São Paulo/SP, Brazil
machadoi@usp.br

Francisco Guilhermo Briones Castilho*
Pontificia Universidad Católica de Valparaíso, Department of Mechanical Engineering, #2950, Valparaíso, Chile
francisco.briones@usp.br

Abstract. *Although cemented carbide is a cutting tool widely used in machining, mechanical and thermal cracks may happen owing to lack of fracture toughness. Functionally Graded Materials (FGM) are composites made of two or more different materials tailored in a gradient form. Cemented carbide and high-speed steel are two important and distinct groups of cutting tool materials. For producing a cemented carbide – high-speed steel FGM, these materials were studied firstly as a single homogeneous composite to understand their microstructure behaviour and sintering parameters influence. Therefore, this work aims to evaluate physical and mechanical properties of a cemented carbide – high-speed steel composite with TiC addition and compare them with those of a commercial homogenous cemented carbide tool. For this, cemented carbide (particle size 1.5 µm), high-speed steel (50 µm) and TiC (0.8 µm) powders were sintered varying the TiC volume fraction from 5 to 35% at 1200ºC, under uniaxial pressure of 20 MPa and 2.2 MPa, using the technique of pulsed electric current sintering (PECS). The physical property, relative density, was determined based on the Archimedes principle. The mechanical properties, hardness and fracture toughness were conducted using a Vickers indenter. The results showed a great influence of the sintering pressure on the relative density and, consequently, on the mechanical properties. For the 5% TiC sample sintered at 20 MPa, the relative density was 97.8%, close to the commercial cemented carbide, 98.1%. Considering mechanical properties, the 5% TiC sample obtained the Vickers hardness number of 1242±62 HV and fracture toughness of 12.4±1.3 MPa.m$^{1/2}$, whereas the commercial sample obtained 1284±176 HV and 13.0±1.3 MPa.m$^{1/2}$. For samples sintered at 2.2 MPa with TiC addition of 15 to 35%, loss of relative density and mechanical properties were observed as the volume fraction of TiC increased. Except for 15% TiC, which attained higher fracture toughness 13.3±1.0 MPa.m$^{1/2}$. In this case, the porosity may have changed the fracture mode. In addition, from 25% TiC sample, the amount of iron segregation in the microstructure decreased. The results showed the importance of applying pressure during sintering to achieve the necessary relative density and mechanical properties. Furthermore, it is desirable to control the TiC content in the microstructure to avoid iron segregation and, consequently, residual stress.*

Keywords: *cemented carbide, sintering, density, hardness, fracture toughness*

1. INTRODUCTION

Sintering is a thermal treatment for bonding powder particles into a coherent solid structure via transport mass phenomena that occur at an atomic level. The bonding leads to improved strength and a lower system energy (German, 1996). Pulsed Electric Current Sintering (PECS), also known as Spark Plasma Sintering (SPS), is a current sintering technique that has gained prominence for being an advanced method that allows sintering materials in a short period by charging powders with electrical current and mechanical pressure simultaneously (Udupa *et al.*, 2014; Gillia and Caillens, 2011). According to Tokita (2000) and Orrù *et al.* (2009), PECS has been used for sintering advanced materials, such as Functionally Graded Materials (FGMs).

FGM provides a solution to many advanced applications, in which two or more materials are put together in a gradient which may be continuous or stepwise (Mott and Evans, 1999; Ma and Tan, 2001). It has gained attention in the materials field because of its potentially universal applicability, such as combining dissimilar functions or properties from different materials into a single element (Kawasaki and Watanabe, 1997; Myamoto *et al*., 1999).

Cemented carbide (CC) and high-speed steel (HSS) are two important cutting tool materials. Cemented carbide is characterised by fine tungsten carbide (WC) particles, which are hard and consequently wear resistant; however, they are brittle and susceptive to thermal and/or mechanical cracks. Fracture toughness is obtained from the metallic binder, cobalt (Co), which is ductile and in minor content (Upadhyaya, 2001; Eriksson *et al.*, 2013). High-speed steel is a complex iron-based alloy of carbon, chromium, vanadium, molybdenum, tungsten and cobalt. This cutting tool material is extensively used to manufacture drills, mills, threads, broaches, etc. (Bayer and Becherer, 1989; Chaus *et al.*, 2019). Braschi *et al.* (2017) developed a FGM compound of cemented carbide and high-speed steel. They observed segregations containing Fe and V due to mass transport events from sintering.

Thus, the aim of this work is to study the effect of adding different volume fractions of TiC into a composite of cemented carbide and high-speed steel to develop a FGM later. Samples were sintered by PECS. Relative density, hardness and fracture toughness were evaluated as well as compared to commercial cemented carbide.

2. METHODOLOGY

The composite cemented carbide (CC) + high-speed steel (HSS) contained volume fraction of 60%CC and 40%HSS. Titanium carbide (TiC) was added to the composite to evaluate microstructure and mechanical property influence; the results were compared with those got from a commercial cemented carbide cutting tool, grade H13A (Sandvik).

2.1 Materials

The materials used were micrometric powders of cemented carbide, grade K20 (Sandvik), high-speed steel, S290 microclean (Böhler) and nanometric powder of TiC (NanoAmor). Table 1 shows the powders characteristics.

Table 1. Characteristics of materials.

Materials	Particle size [µm]	Density [g/cm³]
WC-Co	1.5	14.90
TiC	0.1	4.93
S290	50.0	8.30

TiC is added to avoid segregation of elements and keep the microstructure the most homogeneous possible. Four samples were defined with the common volume fraction of CC and HSS, as aforementioned. The volume fraction of TiC changed for each sample by 5, 15, 25 and 35%. A volume was arbitrated to calculate the samples mass. A precision scale, AD200 model (Marte) with 0.001 g resolution, was used for mass measurements. Table 2 shows volume fractions and mass used.

Table 2. Volume fraction of TiC and cemented carbide + high-speed steel for each sample.

Sample	Volume fraction of TiC [%]	Volume fraction of CC + HSS [%]	TiC Mass [g]	CC + HSS Mass [g]	Total Mass [g]
CCHSS-5TiC	5	95	0.277	13.103	13.380
CCHSS-15TiC	15	85	0.832	11.724	12.556
CCHSS-25TiC	25	75	1.387	10.344	11.731
CCHSS-35TiC	35	65	1.941	8.965	10.906

Next, the powders of each sample were separated and packaged in bottles. The powders were mixed in a liquid environment of isopropyl alcohol for 37 hours in a Wagner type mixer (New Lab). Milling elements of cemented carbide in a mass ratio of 2:1 in relation to powder were used. After that, the powders were dried in a laboratory drying oven, NL80/42 model (New Lab) for 24 hours and mechanically deagglomerated for 6 hours.

2.2 Sintering

The samples were processed by Pulsed Electric Current Sintering (PECS) technique using a 1050 machine (SPS Syntex Inc.), which conducted thermal and loading cycles automatically from a PID controller. The loose powders were manually placed in a graphite die, grade MBIS60X (Morganite). The internal wall of the graphite die was wrapped with a graphite sheet, Grafoil GTB (Morganite), to prevent adhesion among the powders, punches, and die wall. The powder

masses were measured using the precision scale, AD200 model (Marte). The graphite die was assembled between upper and lower machine punches into the vacuum chamber, see Figure 1.

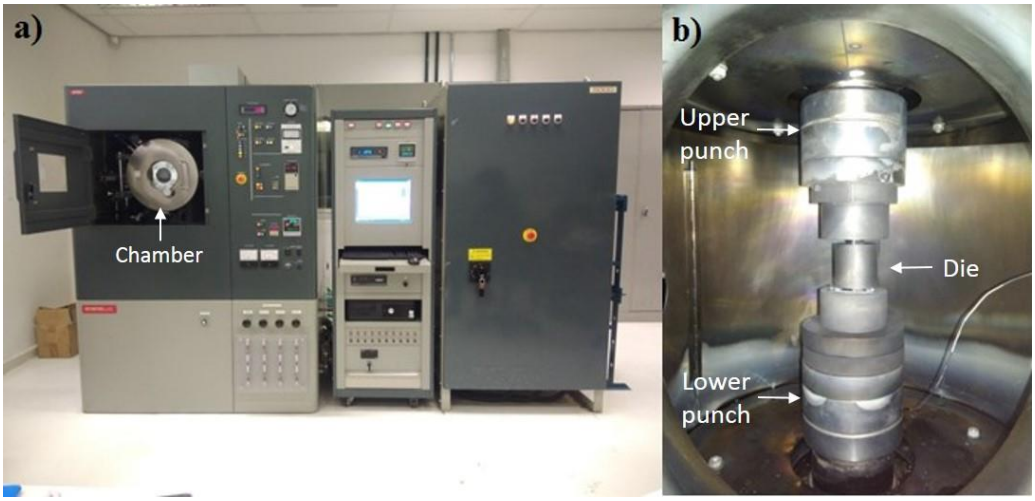

Figure 1. Sintering process. (a) Pulsed electric current sintering machine, 1050 model (SPS Syntex Inc.); (b) Assembly of graphite die into the vacuum chamber.

Table 3 presents the sintering parameters by PECS for each sample performed. The heating and cooling rates were 100ºC/min and 80ºC/min. The dwell time at a sintering temperature of 1200ºC was 6 minutes.

Table 3. PECS sintering parameters.

Sample	Temperature [°C]	Pressure [MPa]	Atmosphere
CCHSS-5TiC	1200	20.0	Vacuum
CCHSS-15TiC	1200	2.2	Vacuum
CCHSS-25TiC	1200	2.2	Vacuum
CCHSS-35TiC	1200	2.2	Vacuum

The sintering temperature was defined based on the literature (Zhao *et al.*, 2008; Carneiro *et al.*, 2011), previously experience with work materials, in addition to HSS austenitising around 1200ºC. The CCHSS-5TiC was sintered with uniaxial pressure of 20 MPa, while CCHSS-15 to 35TiC must be considered samples sintered without pressure. The pressure value of 2.2 MPa is the minimum value for practical machine functioning.

2.3 Metallographic Preparation and Microscopy

Sintered samples had the transversal section sectioned using a precision saw, IsoMet 1000 (Buehler), with sectioning blade 15HC (Buehler). One-half part was used for density analysis, another for mechanical property evaluation. After that, the samples were mounted in a phenolic thermoset resin using a manual compression-mounting machine EFD30 (Fortel). The samples were ground manually using SiC powders with grit sizes of 400, 600, and 1000. Then, they were polished using Nylon PSA cloths with diamond pastes (MetaDi II) having particle sizes of 15, 6, and 1 μm. Grinding and polishing steps were performed on a table-top unit PLFDV (Fortel).

After preparation, the microstructure analysis was performed in an optical microscope, Eclipse MA200 inverted microscope (Nikon), and scanning electron microscope, JSM 7100FT (JEOL) with energy-dispersive X-ray spectroscopy detector conjugated, X-MAX (Oxford). The former was used mainly for measuring the indentation sizes and cracks from mechanical tests. The latter was used to show the main elements from segregations in the microstructure.

2.4 Density

Relative density was determined based on ISO 10545-3:2018. For this procedure, a precision scale AD200 (Marte) with hydrostatic kit was used. First, the samples were heated in distilled water at boiling temperature for two hours, and later cooled immersed until room temperature. Next, their suspended mass (m_3) was measured using the Archimedes' apparatus (hydrostatic kit). The mass measurements were performed using a spit type digital thermometer, model TM879 (Equitherm). Impregnated with water mass (m_2) was measured removing the excess water from the surfaces before putting the samples into the precision scale. Finally, the dry mass (m_1) of samples was measured, after keeping them for

24 hours at 110ºC into a laboratory drying oven, NL80/42 model (New Lab). For each sample 15 measurements were made to determine the experimental density (ρ_{exp}) shown in Eq. (1). The distilled water density (ρ_{H_2O}) was calculated by Eq. (2). T is distilled water temperature [ºC]. Theoretical density (ρ_t) was estimated by the inverse rule of mixtures (German and Park, 2008), Eq. (3), using materials density from Table 1 and constituents weight percentage ($wt\%$). Relative density (ρ_{rel}) was determined according to Eq. (4).

$$\rho_{exp} = \frac{m_1}{m_2 - m_3}\rho_{H_2O} \text{ [g/cm}^3\text{]} \quad (1)$$

$$\rho_{H_2O} = 1.0017 - 0.0002135T \text{ [g/cm}^3\text{]} \quad (2)$$

$$\frac{1}{\rho_t} = \frac{wt\%_{WC-Co}}{\rho_{WC-Co}} + \frac{wt\%_{HSS}}{\rho_{HSS}} + \frac{wt\%_{TiC}}{\rho_{TiC}} \text{ [1/g/cm}^3\text{]} \quad (3)$$

$$\rho_{rel} = \frac{\rho_{exp}}{\rho_t}100 \text{ [\%]} \quad (4)$$

2.5 Vickers Hardness and Fracture Toughness

The mechanical properties (hardness and fracture toughness, K_{IC}) were conducted using a Vickers indenter. The Wolpert hardness tester with capacity of 15.625 to 250 kgf was used. Knowing that the workpiece material is a composite containing a major content of cemented carbide, and this has ceramic characteristics, too, the Vickers hardness test was carried out based on ASTM E92-17:2017 and ASTM C1327-15:2019 standards. The spacing of indentations in cracking condition was at least 5 times the length of the cracks. The results were obtained from 12 indentations performed in each sample. The Vickers hardness number (HV) was calculated according to Eq. (5), (P) loading in kilogram-force and (d) average length of the two diagonals in milimitres.

$$HV = 1.8544(P/d^2) \quad (5)$$

Fracture toughness for plane-strain in mode I of loading (K_{IC}) was evaluated by means of Eq. (6). (E) is the elasticity modulus [GPa], (H) is the hardness value [GPa], (F) is the load applied [N], and (c) is the crack extension [m] (Meyers and Chawla, 2009).

$$K_{IC} = 0.016(E/H)^{1/2}\ \left(F/c^{3/2}\right) \text{ [MPa.m}^{1/2}\text{]} \quad (6)$$

The elasticity modulus of samples ($E_{samples}$) was estimated from the sum of the product of elasticity modulus of each constituent by the corresponding volume fraction, Eq. (7) and (8) (Lanhe, 2004; German and Park, 2008). E_{CC-HSS} is the elasticity modulus of cemented carbide (E_{CC}) multiplied by the volume fraction of 60% ($v\%$), plus the elasticity modulus of high-speed steel (E_{HSS}) multiplied by the volume fraction of 40% ($1 - v\%$). Thus, $E_{samples}$ corresponds to the product of E_{CC-HSS} by its corresponding volume fraction ($v'\%$), plus the product of the elasticity modulus of TiC (E_{TiC}) by its volume fraction ($1 - v'\%$).

$$E_{CC-HSS} = E_{CC}.v\% + E_{HSS}.(1 - v\%) \quad (7)$$

$$E_{samples} = E_{CC-HSS}.v'\% + E_{TiC}.(1 - v'\%) \quad (8)$$

3. RESULTS AND DISCUSSION

3.1 Microscopy and Density

Optical microscopy of CCHSS-TiC samples are shown in Figure 2. Analyzing the micrographs, it was noted that CCHSS-5TiC and CCHSS-15TiC samples presented a dark phase in the shape of veins and globular, respectively, as also observed by Braschi *et al.* (2017). The vein shape is due to the uniaxial sintering pressure, while the spheroidal shape is due to its absence. For CCHSS-25TiC, the microstructure is more homogeneous with some agglomerates of WC; however, without a large presence of dark phase. The same can be noted for CCHSS-35TiC sample; nevertheless, some agglomerates are observed here, surrounded by a second phase. The microstructure features are highlighted with an arrow.

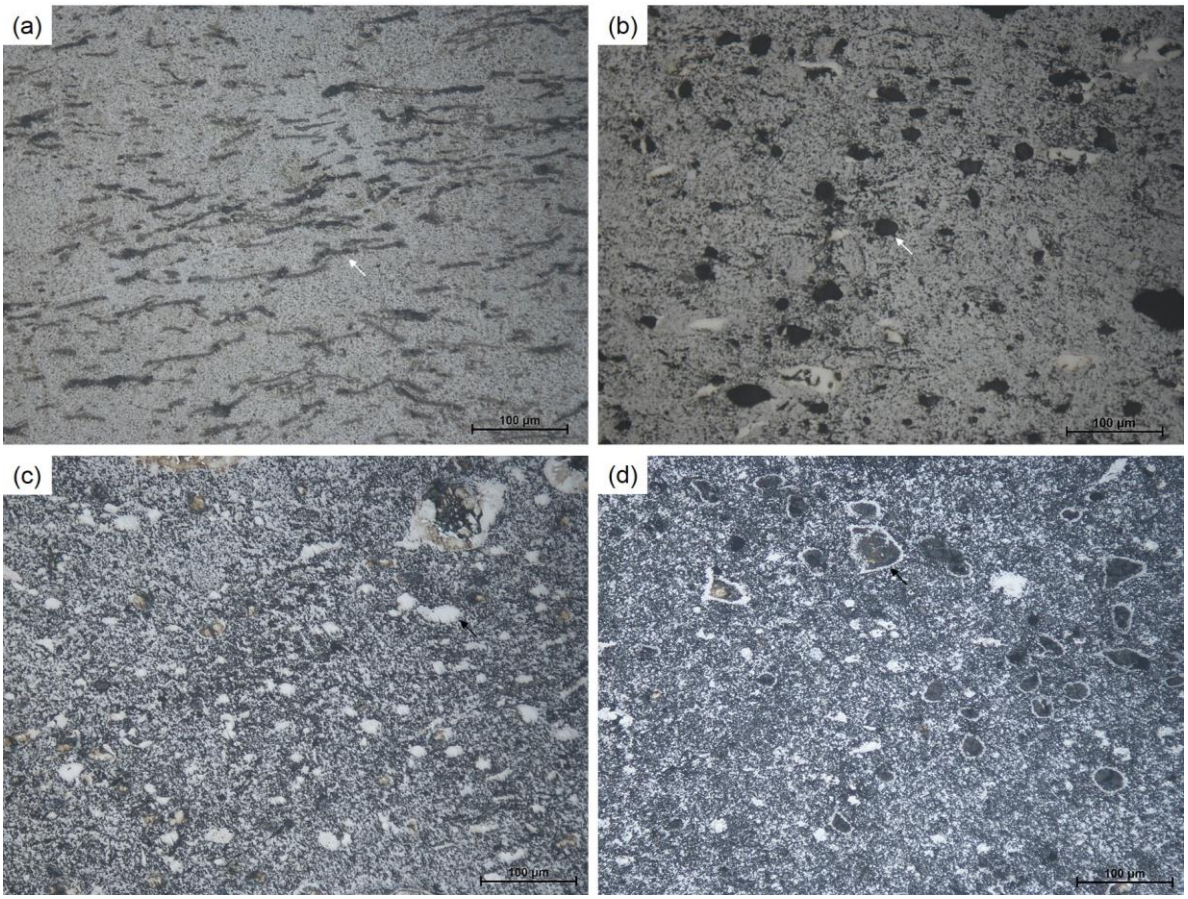

Figure 2. Optical micrographs. (a) CCHSS-5TiC; (b) CCHSS-15TiC; (c) CCHSS-25TiC; (d) CCHSS-35TiC.

EDS analysis of dark phase for CCHSS-5TiC and CCHSS-15TiC allowed identifying that its chemical content was mainly Fe and in minor level Co, surrounded by V and Ti, see Figure 3(a). As aforementioned, the presence of this phase was lower in CCHSS-25TiC and CCHSS-35TiC. The core content consisted mainly of Fe and Co, surrounded by a Ti content higher than V, Figure 3(b). As observed, all samples had high level of W in the matrix and the TiC content influenced the microstructural changes.

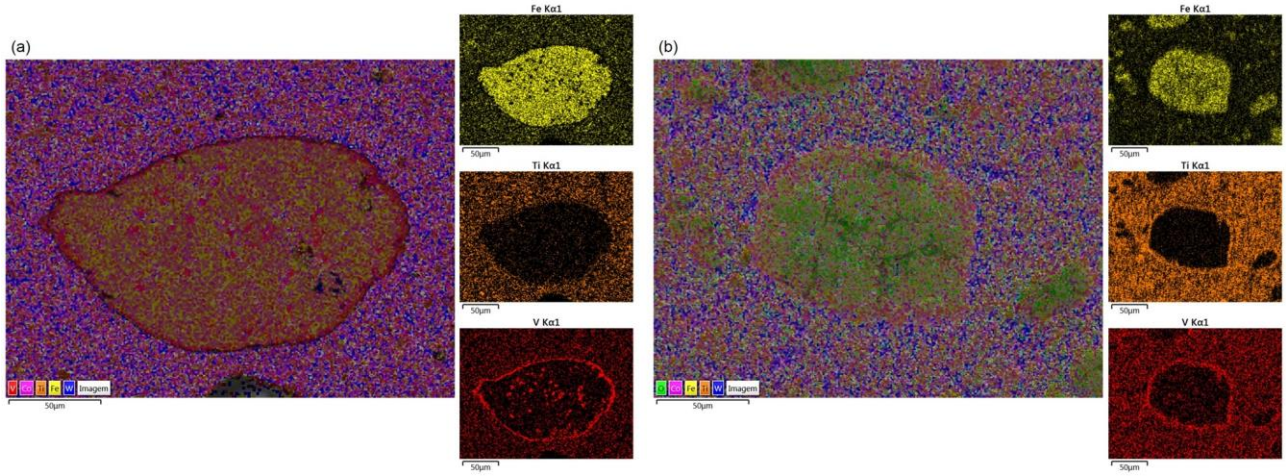

Figure 3. EDS map. (a) CCHSS-15TiC; (b) CCHSS-35TiC.

The results for the relative density of samples are shown in Table 4. The CCHSS-5TiC sample sintered with uniaxial pressure of 20 MPa had the highest relative density, close to commercial cemented carbide density 98%. Braschi *et al.* (2017) reached relative densities around 96% under pressure of 40 MPa and without TiC addition. It was observed that increasing the TiC content from 15 to 35% produced a slight drop in relative density for samples sintered under the same

conditions, as shown in Figure 4. The lack of pressure changed the thermodynamics of mass transport, making the sintering less effective, contributing to the non-dilution of the carbides into the iron, soon their detachment occur from the matrix and, consequently, aided to increase the porosity. It is evaluated that the pressure applied during the sintering by PECS had a great influence on the relative density for CCHSS-5TiC compared to other heat-treated samples without pressure. The standard deviation difference between commercial CC and CCHSS-TiC samples may be related to different powder particle sizes of and sintering techniques used. However, in both cases the deviation is low. The presence of pores is expected to influence the mechanical properties for CCHSS-15TiC to CCHSS-35TiC samples.

Table 4. Density evaluation for sintered samples and commercial cemented carbide.

Sample	ρ_t [g/cm³]	ρ_{exp} [g/cm³]	ρ_{rel} [%]	ρ_{rel} standard deviation [%]
Commercial CC	14.90	14.65	98.12	1.27
CCHSS-5TiC	11.89	11.62	97.77	0.49
CCHSS-15TiC	11.16	9.05	81.07	0.30
CCHSS-25TiC	10.43	8.12	77.83	0.22
CCHSS-35TiC	9.69	7.38	76.12	0.28

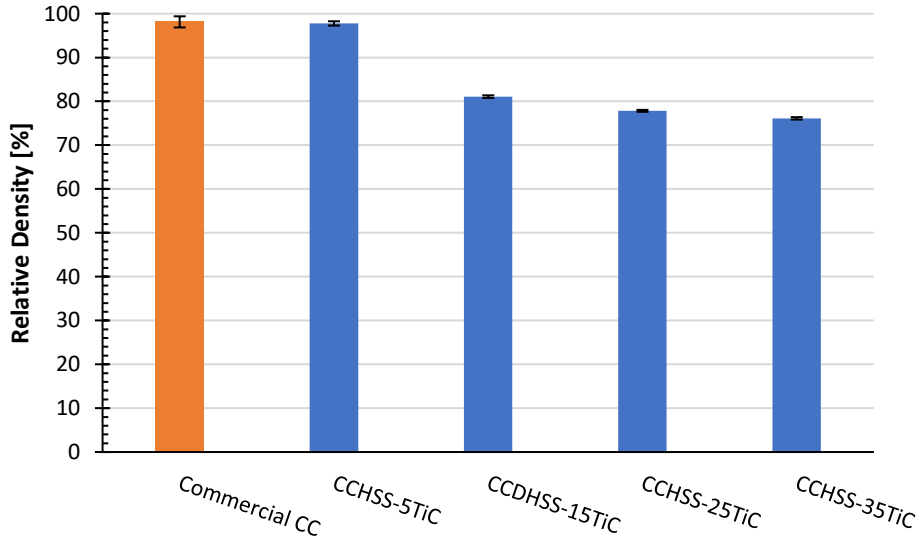

Figure 4. Relative density comparison among samples sintered by PECS and commercial cemented carbide.

3.2 Mechanical Properties

According to German (1996), the relative density is directly related to the properties of the sintered material. The results of Vickers hardness number and fracture toughness (K_{IC}) are shown in Table 5.

Table 5. Vickers hardness number and fracture toughness (K_{IC}).

Sample	ρ_{rel} [%]	Vickers Hardness [HV]	Elasticity Modulus [GPa]	K_{IC} [MPa.m$^{1/2}$]
Commercial CC	98.12	1284±176	664	13.0±1.3
CCHSS-5TiC	97.77	1242±62	474	12.5±1.3
CCHSS-15TiC	81.07	589±88	471	13.3±1.0
CCHSS-25TiC	77.83	453±73	469	6.8±0.9
CCHSS-35TiC	76.12	361±37	466	5.0±0.2

Figure 5 shows the influence of relative density on Vickers hardness. When the samples are closer to full density (commercial CC and CCHSS-5TiC), the Vickers hardness for both is similar, even if the composite has 40% in volume of HSS. The addition of carbides, such as TiC, VC, Cr_3C_2, ZrC, NbC or TaC to the powder mixture inhibits the growth of WC grains during sintering, increasing the hardness, and, consequently, the wear resistance (Hayashi *et al.*, 1972; Weidow and Andrén, 2001). Comparing CCHSS-5TiC with CCHSS-15TiC (sintered samples with and without uniaxial pressure), the lack of pressure causes an increase in porosity, dramatically decreasing hardness. Analysing the results for

samples sintered in the same conditions (CCHSS-15TiC to CHSS-35TiC), increasing the TiC content, the relative density is observed to decrease, as well as the hardness. Property loss occurs because porosity decreases the material resistance to penetration.

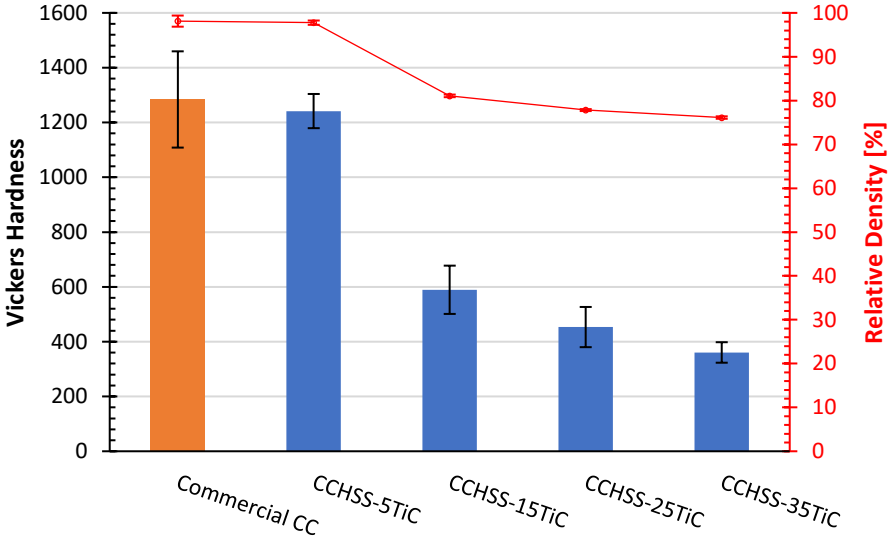

Figure 5. Relation between density and Vickers hardness.

Figure 6 shows the influence of relative density on fracture toughness (K_{IC}). For dense samples (commercial CC and CCHSS-5TiC), the K_{IC} values are notedly similar to each other and close to the literature (Upadhyaya, 2001). When comparing CCHSS-5TiC with CCHSS-15TiC, there is an increase in K_{IC} mean value, even with the drop in relative density. According to Meyers and Chawla (2009) and Kim *et al.* (2016), some level of porosity is able to absorb fracture energy, changes the fracture mode, besides influencing the elasticity modulus increasing the K_{IC}. Below 80% of relative density, increasing TiC content from 25 to 35% has a drastic decrease in K_{IC}. For dense samples, the increase of TiC content is supposed to increase K_{IC} to some extent, as the carbide might act as a barrier to the dislocation movement. In turn, to some extent of TiC contents, the mechanical behaviour may change, increasing hardness and decreasing K_{IC}.

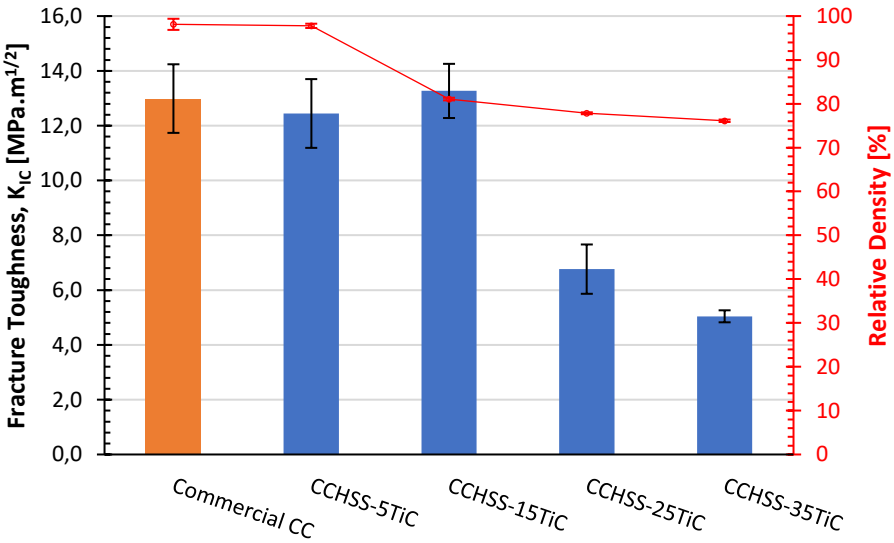

Figure 6. Relation between density and fracture toughness.

4. CONCLUSIONS

The microstructure was observed to change with TiC addition. A pressure applied of 20 MPa is enough to provide dense CCHSS composites. However, care must be taken to avoid the liquid phase leaking from die. When increasing the TiC content from 15 to 35% in the same sintering conditions, a decrease in relative density was noted. Therefore, with

higher TiC content higher input of temperature, pressure and/or sintering time should be used to achieve densification. Relative density has a large influence on the Vickers hardness. Thus, the increase in porosity causes property loss. Density also influenced the fracture toughness results. An increase in K_{IC} was verified for 18% of porosity (CCHSS-15TiC). However, for porosity levels above 20%, there was a drastic drop in the property. These results contribute to a further development towards achieving a successful FGM compound of CC and HSS.

5. ACKNOWLEDGEMENTS

The authors would like to thank Capes and FAPES (Grant 083/2019 and 144/2020) for providing financial support.

6. REFERENCES

ASTM C1327-15, 2019, *American Society for Testing and Materials*. Standard Test Method for Vickers Indentation Hardness of Advanced Ceramics, ASTM International.

ASTM E92-17, 2017, *American Society for Testing and Materials.* Standard Test Methods for Vickers Hardness and Knoop Hardness of Metallic Materials, ASTM International.

Bayer, A.M. and Becherer, B.A., 1989. "High-speed tool steels". *ASM Handbook: Machining. ASM International*, v. 16, p. 944.

Braschi, G.; Eiras, J.A.; Barbosa, P.A.; De Rossi, W., and Carneiro, M.B., 2017. "Material development in functional grading of carbide and high-speed steel for cutting tool (in Portuguese)". In *Proceedings of the 9th Brazilian Congress on Manufacturing Engineering – COBEF 2017*. ABCM. Joinville, Santa Catarina, Brazil.

Carneiro, M.B.; Machado, I.F., and Rodrigues, D., 2011. "Analysis of Sintering Parameters by SPS on Cemented Carbide". *Advanced Materials Research*, Vol. 223, p. 579-587.

Chaus, A.S.; Bracík, M.; Sahul, M., and Dománková, M., 2019. "Microstructure and properties of M2 high-speed steel cast by the gravity and vacuum investment casting". *Vacuum*, 162, p. 183-198.

Eriksson, M.; Radwan, M., and Shen, Z., 2013. "Spark plasma sintering of WC, cemented carbide and functional graded materials". *Int. Journal of Refractory Metals and Hard Materials*, 36, p. 31-37.

German, R.M., 1996. *Sintering theory and practice*. New York: John Wiley & Sons Inc., 550 p.

German, R.M. and Park, S.J., 2008. *Handbook mathematical relations in particulate materials processing: ceramics, powder metals, cermets, carbides, hard materials, and minerals*. New York: John Wiley & Sons, 419 p. 2008.

Gillia, O. and Caillens, B., 2011. "Fabrication of a material with composition gradient for metal/ceramic assembly". *Powder Technology*, Vol. 208, p. 355-366.

Hayashi, K.; Fuke, Y., and Suzuki H., 1972. "Effects of addition carbides on the grain size of WC–Co alloy". *Journal of the Japan Society of Powder and Powder Metallurgy*, Vol. 19, p. 67–71.

ISO 10545-3, 2018, *International Organization for Standardization*. Ceramic tiles – Part 3: Determination of water absorption, apparent porosity, apparent relative density and bulk density.

Kawasaki, A. and Watanabe, R., 1997. "Concept and P/M fabrication of functionally gradient materials". *Ceramics International*, V. 23, p. 79-83.

Kim, Y.; Jo, H.; Allen, J.L.; Choe, H.; Wolfenstine, J., and Sakamoto, J., 2016. "The effect of relative density on the mechanical properties of hot-pressed cubic Li7La3Zr2O12". *Journal of the American Ceramic Society*, Vol. 99, p. 1367-1374.

Lanhe, W., 2004. "Thermal buckling of a simply supported moderately thick rectangular FGM plate". *Elsevier Composite Structures*, p. 211-218.

Ma, J. and Tan, G.E.B., 2001. "Processing and characterization of metal-ceramics functionally gradient materials". *Journal of Materials Processing Technology*, v. 113, p. 446-449.

Meyers, M.A. and Chawla, K.K., 2009. *Mechanical behaviour of materials*. Cambridge: Cambridge University Press.

Miyamoto, Y.; Kaysser, W.A.; Rabin, B.H.; Kawasaki, A., and Ford, R.G., 1999. *Functionally graded materials: design, processing and applications*. New York: Springer, 330 p.

Mott, M. and Evans, J.R.G., 1999. "Zirconia/alumina functionally graded material made by ceramic ink jet printing". *Materials Science and Engineering A*, V. 271, p. 344-352.

Orrù, R.; Licheri, R.; Locci, A.M.; Cincotti, A., and Cao, G., 2009. "Consolidation/synthesis of materials by electric current activated/assisted sintering". *Materials Science and Engineering R*, V. 63, p. 127-287.

Tokita, M., 2000. "Mechanism of spark plasma sintering". In *Proceedings of 2000 Powder Metallurgy World Congress*, Kyoto, Japan, p. 729-732.

Udupa, G.; Rao, S.S., and Gangadharan, K.V., 2014. "Functionally Graded Composite Materials: An Overview". *Procedia Materials Science*, v. 5, p. 1291-1299.

Upadhyaya, G.S., 2001. "Materials Science of cemented carbides – an overview". *Materials and Design*, v. 22, p. 483-489.

Weidow, J., and Andrén, H.O., 2011. "Grain and phase boundary segregation in WC-Co with TiC, ZrC, NbC or TaC additions". *Int. Journal of Refractory Metals and Hard Materials*, Vol. 29, p. 38-43.

Zhao, S.; Song, X.; Zhang, J., and Liu, X., 2008. "Effects of scale combination and contact condition of raw powders on SPS sintered near-nanocrystalline WC–Co alloy". *Materials Science and Engineering A*, Vol. 473, p. 323-329.

7. RESPONSIBILITY NOTICE

The authors are the only responsible for the printed material included in this paper.